No need for dark matter: resolved kinematics of the ultra-diffuse galaxy AGC 114905

Pavel E. Mancera Piña [1,2]★ Filippo Fraternali [1] Tom Oosterloo [1,2] Elizabeth A. K. Adams [1,2] Kyle A. Oman [3] and Lukas Leisman [4,5]

[1] *Kapteyn Astronomical Institute, University of Groningen, Landleven 12, NL-9747 AD Groningen, the Netherlands*
[2] *ASTRON, Netherlands Institute for Radio Astronomy, Oude Hoogeveensedijk 4, NL-7991 PD Dwingeloo, the Netherlands*
[3] *Institute for Computational Cosmology, Department of Physics, Durham University, South Road, Durham DH1 3LE, UK*
[4] *Department of Physics and Astronomy, Valparaiso University, 1610 Campus Drive East, Valparaiso, IN 46383, USA*
[5] *Department of Astronomy, University of Illinois, 1002 W. Green St., Urbana, IL 61801, USA*

ABSTRACT

We present new H I interferometric observations of the gas-rich ultra-diffuse galaxy AGC 114905, which previous work, based on low-resolution data, identified as an outlier of the baryonic Tully–Fisher relation. The new observations, at a spatial resolution ∼2.5 times higher than before, reveal a regular H I disc rotating at about 23 km s^{-1}. Our kinematic parameters, recovered with a robust 3D kinematic modelling fitting technique, show that the flat part of the rotation curve is reached. Intriguingly, the rotation curve can be explained almost entirely by the baryonic mass distribution alone. We show that a standard cold dark matter halo that follows the concentration–halo mass relation fails to reproduce the amplitude of the rotation curve by a large margin. Only a halo with an extremely (and arguably unfeasible) low concentration reaches agreement with the data. We also find that the rotation curve of AGC 114905 deviates strongly from the predictions of modified Newtonian dynamics. The inclination of the galaxy, which is measured independently from our modelling, remains the largest uncertainty in our analysis, but the associated errors are not large enough to reconcile the galaxy with the expectations of cold dark matter or modified Newtonian dynamics.

Key words: galaxies: dwarf – galaxies: formation – galaxies: irregular – galaxies: kinematics and dynamics – dark matter.

1 INTRODUCTION

The properties, origin, and formation mechanisms of ultra-diffuse galaxies (UDGs) have been widely discussed in the last years. UDGs (van Dokkum et al. 2015) are low surface brightness galaxies (e.g. Impey, Bothun & Malin 1988, see also discussion in Conselice 2018) with an extended light distribution. At fixed stellar mass or luminosity, UDGs have significantly larger effective radii than the 'classical' dwarf galaxy population (e.g. Mihos et al. 2015; van Dokkum et al. 2015; Mancera Piña et al. 2019a; Chamba, Trujillo & Knapen 2020).

UDGs are mostly found by number in massive galaxy clusters, but they are also present in galaxy groups, in the field, and even in voids (e.g. van der Burg, Muzzin & Hoekstra 2016; Leisman et al. 2017; Román & Trujillo 2017; Román et al. 2019; Mancera Piña et al. 2019a; Barbosa et al. 2020; Karunakaran et al. 2020). The ubiquity of UDGs across different environments indicates that even if some of them form due to environmental processes, this is not the case for all UDGs, and they can also form due to their own internal processes. The population of UDGs is likely a mixed bag of galaxies with similar sizes and surface brightness, but perhaps multiple formation mechanisms.

The above idea seems confirmed by a number of results from semi-analytic models and hydrodynamics simulations that produce UDG-like simulated galaxies based on different physical processes. On the one hand, different authors report that classical dwarf galaxies can become UDGs (i.e. increase their size and likely decrease their surface brightness) due to cluster pre-processing phenomena such as tidal striping and tidal heating (Carleton et al. 2019; Sales et al. 2020; Tremmel et al. 2020). On the other hand, it has also been suggested that internal processes can explain the optical properties of UDGs. Amorisco & Loeb (2016) proposed a model where UDGs form due to a higher than average dark matter angular momentum, which then gives rise to an extended stellar effective radius (see also Rong et al. 2017). Here, it is worth mentioning that even if UDGs inhabit normal dark matter haloes, they could still have a higher than average retained fraction of stellar specific angular momentum (Posti et al. 2018; Mancera Piña et al. 2020). Another idea is that UDGs are dwarfs that became larger due to feedback-driven outflows, which change the dark matter and baryonic potential and allow the stars to migrate to more external orbits, increasing their effective radius (Di Cintio et al. 2017; Chan et al. 2018). It has also been argued that the expansion of the stellar orbits can be the result of massive mergers at early ($z > 1$) epochs (Wright et al. 2021) or the by-product of very efficient globular cluster feedback (Trujillo-Gomez, Kruijssen & Reina-Campos 2021).

★ E-mail: pavel@astro.rug.nl

While the above models and simulations seem to produce simulated galaxies that match a number of properties of real UDGs, surprising observations of two different populations of UDGs have been more challenging to reproduce. First, it has been found that two gas-poor UDGs (DF-2 and DF-4) near (at least in projection) the galaxy NGC 1052, contain significantly less dark matter than expected based on stellar and globular cluster kinematics (e.g. van Dokkum et al. 2018, 2019; Danieli et al. 2019; Emsellem et al. 2019). While caveats regarding the distance and accuracy of the kinematic tracers used to study these UDGs have been raised (e.g. Laporte, Agnello & Navarro 2019; Trujillo et al. 2019), DF-2 and DF-4 have motivated multiple studies aiming to explain the existence of dark matter free galaxies. The main ideas to explain their existence involve dark matter removing mechanisms such as high-velocity collisions and tidal stripping, or a tidal dwarf origin (Haslbauer et al. 2019; Silk 2019; Montes et al. 2020; Shin et al. 2020; Doppel et al. 2021; Jackson et al. 2021).

The second set of puzzling observations, still very much lacking a quantitative explanation, is related to the H I kinematics of some gas-rich UDGs (sometimes also called H I-bearing UDGs). Using unresolved ALFALFA data (see Haynes et al. 2018), Leisman et al. (2017, see also Jones et al. 2018; Karunakaran et al. 2020) first found that gas-rich UDGs have narrow global H I profiles for their gas mass. Then, Mancera Piña et al. (2019b, 2020) studied a set of six of those gas-rich UDGs with low-resolution (two independent resolution elements per galaxy side) interferometric H I observations. Using a state-of-the-art kinematic modelling fitting technique (^{3D}Barolo; Di Teodoro & Fraternali 2015) to overcome beam smearing effects, they recovered the circular speeds of their galaxies, unveiling two intriguing features. First, that having a baryonic mass a factor 10–100 larger than galaxies with similar circular speed, H I-rich UDGs shift off the baryonic Tully–Fisher relation (BTFR; McGaugh et al. 2000), with the offset from the BTFR correlating with the UDGs optical disc scale lengths. And second, that their dynamical mass within the extent of the H I disc is about the same as their baryonic mass, meaning that the galaxies have very low dark matter fractions within scales as large as 10 kpc. These features suggest that gas-rich UDGs have atypical non-luminous mass distributions, making them a promising population to test dark matter theories. It is also important to stress that these gas-rich UDGs are selected to be fairly isolated (Leisman et al. 2017), and they lie at distances of several tens of Mpc where Hubble flow distances are robust, negating some of the main concerns raised for DF-2 and DF-4.

Given all this, it is important to further characterize the properties of these UDGs, which are apparently gas-rich but also dark-matter poor (at least within the observed radii). One way to do this is by studying their H I rotation curves, as H I provides arguably the best kinematic tracer for disc galaxies, both massive and dwarfs (e.g. Begeman 1987; de Blok et al. 2008; Iorio et al. 2017).

In this work, we present and analyse new, high-resolution interferometric observations of one of these peculiar gas-rich UDGs, AGC 114905. As we will show, the galaxy seems to pose a challenge to the currently favoured galaxy formation framework. This paper is organized in the following way. In Section 2, we describe the main properties of AGC 114905 and we present the data used in this work. In Section 3, we show the kinematic modelling of the galaxy, and in Section 4 the resulting mass models. We discuss our results in Section 5, to then present our conclusions and summary in Section 6.

2 DATA AND PROPERTIES OF AGC 114905

AGC 114905 (01:25:18.60, +07:21:41.11, J2000) lies at a (Hubble-flow) distance $D = 76 \pm 5$ Mpc (Leisman et al. 2017). The stellar distribution of AGC 114905, consists of an exponential disc with a disc scale length $R_d = 1.79 \pm 0.04$ kpc. The left-hand panel of Fig. 1 shows its *r*-band stellar image. The galaxy has a relatively blue colour, $(g - r) = 0.3 \pm 0.1$ (Mancera Piña et al. 2020; Gault et al. 2021). We estimate the stellar mass (M_*) of the galaxy using the mass-to-light–colour relation from Du et al. (2020), which has been recently calibrated using a large sample of low surface brightness galaxies. We obtain $M_* = (1.3 \pm 0.3) \times 10^8$ M$_\odot$; this is slightly smaller than the value used in Mancera Piña et al. (2019b, 2020), owing to the different mass-to-light–colour calibrations.

We gathered H I data of AGC 114905 at different spatial resolutions, obtained with the Karl G. Jansky Very Large Array. Specifically, we collected data from the D-, C- and B-array configurations. Details on the D and C configuration observations (PI: Leisman, ID 17A-210) can be found in Leisman et al. (2017) and Gault et al. (2021). The new B-array observations (PI: Mancera Piña, ID 20A-095) were obtained between 2020 July and October. 40 hours were observed (about 34 hours on-source) and combined with the existing C- and D-array observations. The data reduction was done with the software MIRIAD (Sault, Teuben & Wright 1995) following standard procedures, using a robust weighting of 0.75 to make the final data cube, which results in a cleaned beam of size 7.88 arcsec × 6.36 arcsec. After Hanning-smoothing, our final cube has a rms noise per channel of about 0.26 mJy/beam and a spectral resolution of 3.4 km s^{-1}.

The peak H I column density is 8.4×10^{20} atoms cm^{-2}, and the noise level is 4.1×10^{19} cm^{-2}. The integral flux of the total H I map is 0.73 ± 0.07 Jy km s^{-1}, close to the value of 0.78 Jy km s^{-1} used in Mancera Piña et al. (2019b), although lower than the 0.96 ± 0.04 Jy km s^{-1} reported by Leisman et al. (2017) from unresolved ALFALFA observations. At the distance of AGC 114905, our integral flux yields $M_{HI} = (9.7 \pm 1.4) \times 10^8$ M$_\odot$.[1]

We combine M_{HI} and M_* to obtain the baryonic mass $M_{bar} = 1.33M_{HI} + M_* = (1.4 \pm 0.2) \times 10^9$ M$_\odot$. The factor 1.33 accounts for the presence of helium, and we neglect any contribution of molecular gas, whose mass is expected to be negligible compared to M_{HI} (e.g. Hunter, Elmegreen & Berger 2019; Wang et al. 2020). The galaxy gas fraction $f_{gas} = M_{gas}/M_{bar} \approx 0.9$, ensures that M_{bar} is robust against possible systematics related to M_*, since the main uncertainty in M_{gas} comes from the distance, which is well constrained.

The total H I map of the galaxy is shown in the middle panel of Fig. 1, and also on the left-hand panel with the H I contours overlaid on top of the stellar emission. It is clear that the gas extends well beyond the optical emission, despite UDGs being optically extended. There is also some degree of misalignment between the optical and H I position angles (see also Gault et al. 2021), although the optical morphology is likely affected by bright, patchy star formation regions. The right-hand panel of Fig. 1 shows the surface mass density profiles of the stellar and gaseous discs of AGC 114905. The stellar profile comes from converting our optical surface brightness profiles into mass density using a mass-to-light ratio in the *r* band of 0.47 (Du et al. 2020). The gas profile is obtained using the GIPSY (van der Hulst et al. 1992) task ELLPROF, and converted to mass density using the conversion factor 1 M$_\odot$pc$^{-2} = 1.25 \times 10^{20}$ atoms cm^{-2}. Once this

---

[1]The ALFALFA flux would instead imply $M_{HI} \approx 1.3 \times 10^9$ M$_\odot$, only strengthening the results shown below.
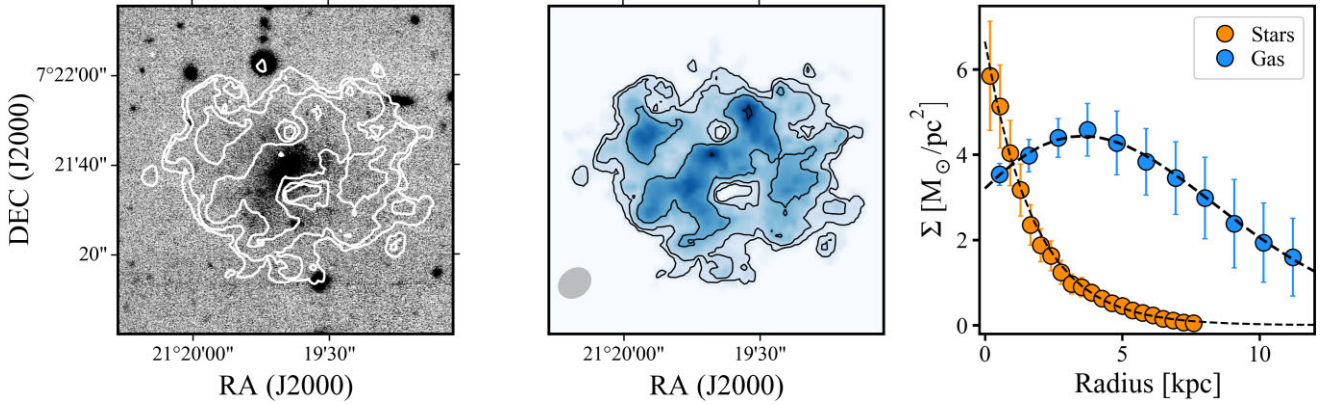
Figure 1. *Left:* Stellar image of AGC 114905 with the total H I contours overlaid. The contours are at 1, 2, 4 × 10²⁰ atoms cm⁻², the noise level is 4.1 × 10¹⁹ atoms cm⁻². *Middle:* Total H I intensity map; contours as in the previous panel. The grey ellipse shows the beam of our data. *Right:* Stellar (orange) and gas (blue, includes helium correction) surface mass density profiles of AGC 114905. The dashed black lines on top show the fits to the distributions used to obtain the stellar and gas circular speeds (see Section 4).

conversion is applied, we multiply by the factor 1.33 to account for the presence of helium.

3 KINEMATICS

In order to obtain reliable kinematic information (rotation velocity and velocity dispersion) for our galaxy, we use the software ³ᴰBarolo (Di Teodoro & Fraternali 2015). As extensively explained in Di Teodoro & Fraternali (2015), Di Teodoro, Fraternali & Miller (2016), and Iorio et al. (2017), ³ᴰBarolo[2] builds 3D realizations of tilted-ring models of a galaxy data cube, which are then convolved with the beam of the observations and compared channel by channel with the real data. This allows for a robust recovery of the rotation curve and gas velocity dispersion, since the method largely mitigates the effects of beam smearing (Bosma 1978; Begeman 1987; Swaters 1999; Di Teodoro & Fraternali 2015).

Before delving into the details and results of our modelling, we will briefly discuss the observed kinematics as well as the derivation of two important geometrical parameters: the position angle and the inclination of the galaxy.

3.1 Velocity field and geometrical parameters

The velocity field (first moment map) of AGC 114905, shown in the top panel of Fig. 2, has the clear kinematic pattern of a regularly rotating disc. The position angle of the velocity field is estimated by trial and error as the angle that maximizes the amplitude of the major-axis position–velocity (PV) diagram (e.g. Mancera Piña et al. 2020). We find a position angle of 89°, as shown in Fig. 2 with a line on top of the velocity field. Our value is similar to the 84° reported in Mancera Piña et al. (2019b, 2020) derived from the less resolved data. If we fit the position angle during our kinematic modelling (see below), we find values between 85° and 92° depending on our initial estimates. The middle (bottom) panel of Fig. 2 shows, in blue background and black contours, the PV diagram along the major (minor) axis of AGC 114905. The major-axis PV shows the typical pattern of

a rotating disc and seems to reach a flat velocity in the outer regions.

While differences of a few degrees in the position angle do not significantly affect the final rotation curve, the inclination of the galaxy is more critical, as small changes at low inclinations can severely affect the value of the deprojected rotation curve. Undoubtedly, the inclination is the main uncertainty in our kinematic modelling and results, and we pay special attention to it. Traditionally, the inclination of high-resolution data can be obtained during the kinematic fitting using the velocity field (e.g. de Blok et al. 2008). However, this method is not particularly robust as it depends on the shape of the rotation curve: for solid-body rotation the iso-contours on the velocity field are parallel, nullifying the power to measure the inclination. Given the above, and following Mancera Piña et al. (2020), we decide to estimate the inclination with an approach that is independent of the kinematics, relying only on the H I map of the galaxy.

Our method works as follows. We use ³ᴰBarolo to build azimuthal models of the galaxy at different inclinations, with these inclinations being drawn from a flat prior distribution between 10° and 80° and sampled using a Markov chain Monte Carlo (MCMC) routine (based on the PYTHON package EMCEE, see Foreman-Mackey et al. 2013). Each model is convolved with the beam of the observations, and its total intensity map is built. We then compare these model intensity maps with the real data, with our MCMC routine minimizing the absolute residuals between model and observed intensity maps. We have tested this method extensively using artificial data cubes matching our resolution and signal-to-noise (S/N), finding it robust and reliable (see also Fraternali et al. 2021). In the end, we find an inclination of 32 ± 3° for AGC 114905, which we adopt as our fiducial value; the posterior distribution is shown in Fig. B1 in Appendix B.

As an extra check, we also estimated the inclination in two other ways.[3] First, using the method described in Mancera Piña et al.

---

[2] https://editeodoro.github.io/Bbarolo/

---

[3] The optical inclination, derived from the optical axial ratio, is around 45°. We do not use this inclination in our analysis as it is not clear if the optical data follows the H I emission (see also e.g. Gault et al. 2021; Kado-Fong et al. 2021), but we provide the value for completeness. Clearly, this inclination would lower the value of the circular speed, strengthening our results.
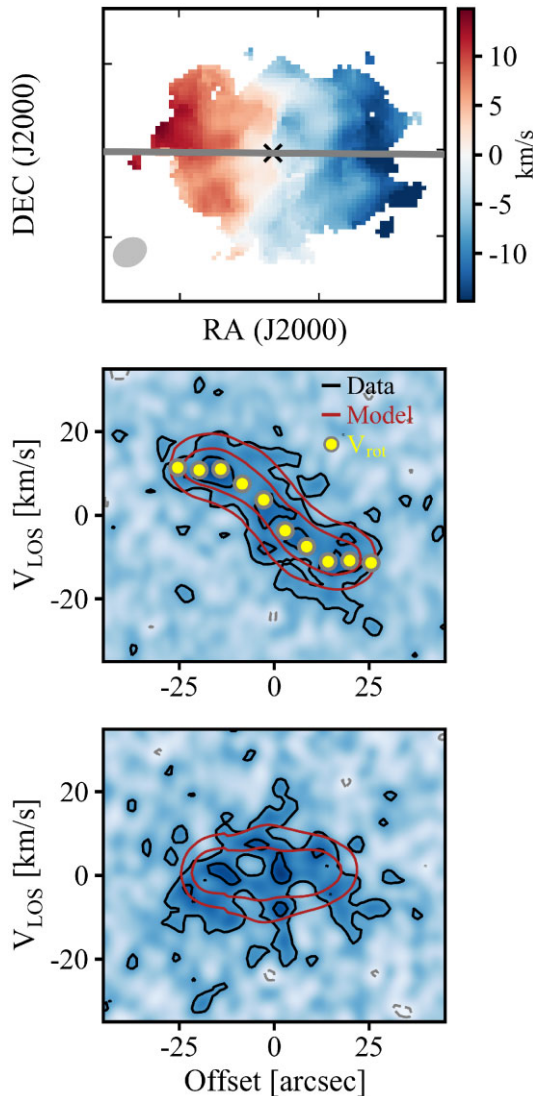
Figure 2. *Top:* Observed velocity field (same physical scale as the total H I map in Fig. 1); the grey ellipse shows the beam of the observations, the grey line the kinematic major axis, and the black cross the kinematic centre. *Middle (Bottom):* Major (minor)-axis PV diagram; data are shown in blue background and black contours (grey for negative values), and the best-fitting ³ᴰBarolo azimuthal model in red contours. The yellow points show the recovered rotation velocities.

(2020), which is equivalent to our method described above but independent of the MCMC sampling. We find an inclination of $34 \pm 5°$, although the quoted uncertainty is just an expected mean value rather than a well-defined statistical uncertainty. Similarly, Mancera Piña et al. (2019b) and Mancera Piña et al. (2020) found an inclination of $33 \pm 5°$ from their lower resolution data. Secondly, we derive kinematic-dependent inclinations. We use both ³ᴰBarolo (fitting the whole data cube) and the GIPSY task ROTCUR (fitting the velocity field). Depending on the exact initial value, mask, and ring separation, both methods find inclinations between $30°$ and $37°$. It is reassuring that despite not being our favoured approaches to measure the inclination, we find these different values consistent with the results of our preferred method. Overall, it is important to highlight that we do not find any evidence favouring inclinations lower than $30°$.

Finally, it is worth mentioning that while deriving the inclination we assume that the H I resides on a razor-thin disc, a significant thickness of the disc would imply a higher inclination than what we have derived due to projection effects (Iorio 2018). From this point of view $32 \pm 3°$ gives a lower limit on the inclination of AGC 114905 (see also Section 5.4). On the other hand, if the gas disc is non-axisymmetric, but instead has some intrinsic elongation, we could be overestimating its inclination. While some simulations suggest this is possible,[4] in what follows we assume that the observed H I total intensity map and velocity gradient correspond to an inclined axisymmetric disc galaxy with gas moving in circular orbits.
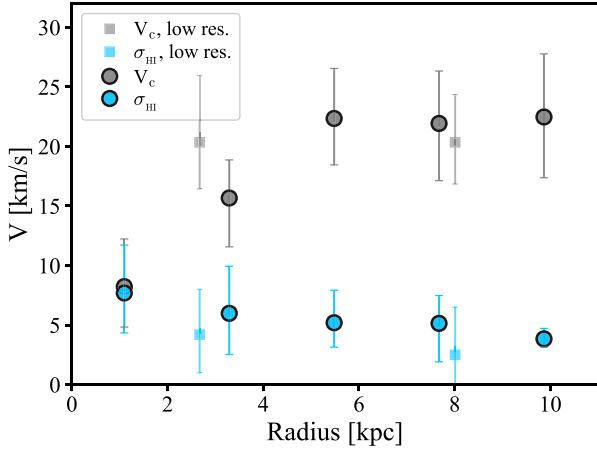
3.2 Kinematic modelling

With the position angle and inclination determined, we proceeded to perform our kinematic modelling with ³ᴰBarolo, leaving as free parameters the systemic velocity (V_{sys}), the rotation velocity (V_{rot}), and the velocity dispersion (σ_{HI}). We fit an azimuthal model and we use a ring separation of 6 arcsec. This represents a minor oversampling of less than 10 percent with respect to the size of the beam along the major axis of the galaxy (6.5 arcsec), allowing us to trace the rotation curve of the galaxy with five, basically uncorrelated, resolution elements per galaxy side. We also check that the rotation velocities obtained using four or five rings (see below) are well consistent with each other.

We first perform an iteration where V_{sys} is a free parameter. The best V_{sys} turns out to be 5435 km s⁻¹, which matches the centre of a Gaussian fit to the global H I profile. For our final model, we keep this V_{sys} fixed and we only fit V_{rot} and σ_{HI}. The final model faithfully reproduces the observations. This can be seen in the middle and bottom panels of Fig. 2, where we compare the PV diagrams of the best-fitting model (red) and data (black). There are some low-S/N features at low velocities ($\lesssim 5$ km s⁻¹) not reproduced, but ³ᴰBarolo closely mimics the overall kinematics of the galaxy. This can also be seen in Appendix A, where we show representative channel maps of AGC 114905 and of our best-fitting model. The resulting rotation curve, uncorrected for inclination, is shown as yellow points overlaid on top of the major-axis PV diagram of Fig. 2, and it is clear that it reaches its flat part well before our outermost radius. To take into account pressure-supported motions, we apply the asymmetric drift correction to our rotation curve (see Iorio et al. 2017), ending up with the circular speed V_c. The correction is found to be very small, contributing less than 2 km s⁻¹ at all radii.

In Fig. 3, we explicitly show the circular speed profile of AGC 114905, as well as its velocity dispersion profile. The uncertainties in V_c include the uncertainties in the inclination, by means of a Monte Carlo sampling approach as detailed in Mancera Piña et al. (2020). The flat part of the circular speed profile has a velocity of $\simeq 23$ km s⁻¹. This, together with the M_{bar} of the galaxy, confirms its position as an outlier of the BTFR. In Fig. 3, we also include for comparison the values for V_c and σ_{HI} obtained in Mancera Piña et al. (2019b, 2020) at lower resolution, showing the good agreement between them and our new determinations. This is important not only for AGC 114905, but for all the UDGs in Mancera Piña et al.

---

[4]Marasco et al. (2018) have reported that about half of the massive dwarf galaxies (60 km s⁻¹ < V_{max} < 120 km s⁻¹, with V_{max} the maximum rotation velocity) in the APOSTLE simulations (Sawala et al. 2015; Fattahi et al. 2016) inhabit dark matter haloes with intrinsic axial ratios $b/a < 0.8$; if the disc of AGC 114905 has a similar intrinsic b/a (i.e. it is an elongated disc instead of an inclined circular disc) its inclination could be as low as $10°$.

Figure 3. Circular speed (grey circles) and velocity dispersion (blue circles) profiles of AGC 114905, as obtained with our kinematic modelling. Squares show previous results obtained at a lower spatial resolution.

(2019b, 2020), as it is a direct validation of the lower resolution results presented previously.

3.3 Local and global disc stability

With a median value of $\sim$5 km s^{-1}, the velocity dispersion σ_{H_I} of AGC 114905 is slightly below the average value in rotation-supported dwarfs ($\sim$8 km s^{-1}, e.g. Iorio et al. 2017) although consistent within the uncertainties. The low values of V_c and σ_{H_I} of our UDG imply a relatively low value of the Toomre parameter $Q_{gas} = \kappa \sigma_{H_I}/(\pi G \Sigma_{gas})$, with κ the epicycle frequency (Toomre 1964). The Q_{gas} profile shows a slight decrease with radius, with a median (mean) value of 0.95 (1.6), after applying a small correction to account for thickness (see Romeo 1994; Romeo & Falstad 2013). The uncertainties are relatively large (typically a factor 2–3), but these values of Q_{gas} suggest that the galaxy could be susceptible to *local* instabilities (see Romeo & Falstad 2013 and references therein for a detailed discussion on the interpretation of Q_{gas}). While these local instabilities may lead to fragmentation and subsequent star formation, observations suggest this is not always the case (Hunter, Elmegreen & Baker 1998; Leroy et al. 2008; Elmegreen & Hunter 2015). The value of Q_{gas} for AGC 114905 is lower on average but consistent within 2σ with the median values of LITTLE THINGS dwarf galaxies (Iorio et al. 2017). Finally, it should be noted that a more detailed calculation that takes into account the gas disc flaring (e.g. Elmegreen & Hunter 2015; Bacchini et al. 2020) would increase the value of Q_{gas}, especially in the outer parts of the disc.

While Q_{gas} is in principle only related to local instabilities, we can also investigate the *global* disc stability of our UDG. The ordered kinematics seen in Fig. 2 and the isolation (see Mancera Piña et al. 2020) of the galaxy strongly suggest an equilibrium state. We further tested this by allowing ^{3D}Barolo to fit radial motions overlaid on the rotation, but we did not find evidence of such radial motions as their amplitude is always consistent with zero within the uncertainties. We also computed the global stability parameter $X_2 = \kappa^2 R/(4\pi G \Sigma_{gas})$ (Toomre 1981), finding a median of 1.2 and with X_2 being smaller than 1 (0.9) only at the outermost radius, suggesting the system is stable against bar instabilities ($X_2 \lesssim 1$ is the instability condition often used for dwarf galaxies, see e.g. Mihos, McGaugh & de Blok 1997; Hidalgo-Gámez 2004).

Overall, these investigations show that it is reasonable to assume that the cold gas in AGC 114905 is in closed orbits tracing its gravitational potential and allowing us to build mass models based on the derived rotation curve.

4 MASS MODELLING

4.1 A baryon-dominated rotation curve

AGC 114905 has a baryonic mass much higher than other dwarf galaxies with similar circular speeds (Iorio et al. 2017; Mancera Piña et al. 2020). It is therefore interesting to see if AGC 114905, like most dwarfs, is dominated by dark matter at all radii.

Prior to obtaining any mass model, we can compare the circular speed profile of the galaxy with the circular speed profile of the baryonic distribution (V_{bar}), which is simply the sum in quadrature of the contributions of the stellar and gas discs, this is $V_{bar}^2 = V_*^2 + V_{gas}^2$. We derive $V_{c,*}$ and $V_{c,gas}$ using the software GALPYNAMICS (Iorio 2018). GALPYNAMICS[5] takes as input the mass density profile of a given component, fitted with an appropriate function (see below), computes its gravitational potential via numerical integration, and returns the associated circular speed.

In the case of the stellar disc, we use an exponential profile with $M_* = 1.3 \times 10^8 \, M_\odot$ and an exponential disc scale length $R_d = 1.79$ kpc; this profile can be compared with the data in Fig. 1. We assume a sech^2 profile along the vertical direction, and a constant thickness $z_d = 0.196 R_d^{0.633} \approx 280$ pc, as found in low-inclination star-forming galaxies (Bershady et al. 2010).

For the gas component (H I plus helium), we fit the density profile with a profile of the form

$$\Sigma_{gas} = \Sigma_{0,gas} e^{-R/R_1} (1 + r/R_2)^\alpha, \tag{1}$$

where $\Sigma_{0,gas}$ is the gas central surface density, R is the cylindrical radius, and R_1, R_2, and α are the fitting parameters (equal to 3.2 $M_\odot$/pc^2, 1.1 kpc, 16.5 kpc and 18, respectively). This profile provides a good fit to the observations, as seen in Fig. 1. For the vertical structure of the gaseous disc we assume a Gaussian profile and a constant vertical scale height $z_d = 250$ pc. It is worth mentioning that the results we show below do not depend significantly on the assumed thickness of the stellar or gaseous discs.

Fig. 4 shows the contribution of V_*, V_{gas}, and V_{bar} to the total V_c of AGC 114905. Remarkably, V_{bar} provides a reasonable description of V_c at all radii. This implies that as opposed to classical dwarf galaxies (e.g. Iorio et al. 2017; Read et al. 2017), the dynamics of AGC 114905, at least within the observed radii extending to about 10 kpc, are baryon-dominated rather than dark-matter dominated. This was already postulated in Mancera Piña et al. (2019b), but it is now confirmed with a well-traced rotation curve.

4.2 Fitting cold dark matter haloes

In our current framework of galaxy formation, we expect every galaxy to be embedded in a cold dark matter (CDM) halo. Because of this, it is relevant to investigate whether or not physically motivated CDM haloes can be consistent with our rotation curve, even if Fig. 4 suggests the absence of a dynamically significant halo in AGC 114905. We aim to find a dark matter halo whose circular speed V_{DM} meets

$$V_c^2 = V_*^2 + V_{gas}^2 + V_{DM}^2. \tag{2}$$

[5]https://gitlab.com/iogiul/galpynamics
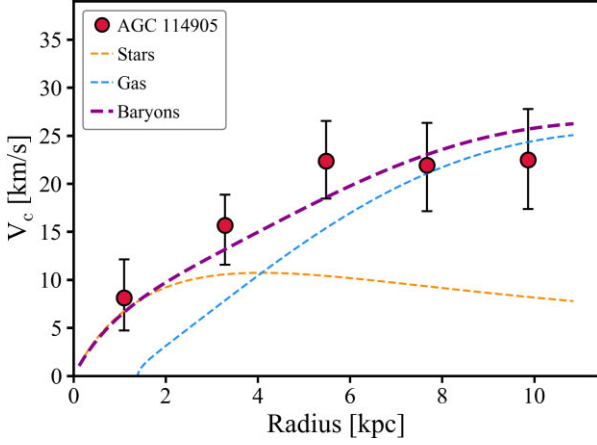
Figure 4. Circular speed profile of AGC 114905 (red points) compared to the contribution expected from stars (orange line), gas (blue line), and baryons (stars plus gas, magenta line).

Dark matter haloes are often described with the so-called NFW profile (Navarro, Frenk & White 1997), whose density as a function of the spherical radius in cylindrical coordinates r ($r = \sqrt{R^2 + z^2}$) is given by

$$\rho_{\mathrm{NFW}}(r) = \frac{4\rho_s}{(r/r_s)(1 + r/r_s)^2}, \tag{3}$$

where r_s is a 'scale radius' and ρ_s is the density at r_s. We will denote the corresponding mass profile as $M_{\mathrm{NFW}}(r)$:

$$M_{\mathrm{NFW}}(< r) = \frac{M_{200}}{\ln(1 + c_{200}) - \frac{c_{200}}{1 + c_{200}}}$$

$$\times \left[\ln\left(1 + \frac{r}{r_s}\right) - \frac{r}{r_s}\left(1 + \frac{r}{r_s}\right)^{-1} \right]. \tag{4}$$

The parameter M_{200} is defined as the mass within a sphere with radius r_{200} within which the average density is 200 times the critical density of the Universe, while the concentration c_{200} is defined as $c_{200} = r_{200}/r_s$.

While NFW haloes provide good descriptions for massive galaxies, this is not the case for dwarf galaxies (see Bullock & Boylan-Kolchin 2017). Therefore, for our UDG, we assume that the dark matter halo is described by a 'CORENFW' profile (Read, Agertz & Collins 2016a), which is an extension of the classical NFW profile that has the flexibility to develop – or not – a core. In Section 5.2, we discuss other halo profiles. The CORENFW profile has been found to fit very well rotation curves of dwarf galaxies, both real and simulated (Read et al. 2016a, b).

The density profile of the CORENFW halo can be written as

$$\rho_{\mathrm{coreNFW}}(r) = f^n \rho_{\mathrm{NFW}}(r) + \frac{n f^{n-1}(1 - f^2)}{4\pi r^2 r_c} M_{\mathrm{NFW}}(r). \tag{5}$$

Here, ρ_{NFW} and M_{NFW} are the above NFW parameters, while f is a function [defined as $f = \tanh(r/r_c)$] that generates a core of size r_c. In principle, r_c can be a fitting parameter, but as discussed in detail by Read et al. (2016a, b, 2017), fixing it to $r_c = 2.94\,R_d$[6] is in good agreement with simulations and observations where r_c is fitted as

---

[6]In principle, $r_c = 1.75\,R_e$, with R_e the half-light radius. For an exponential profile ($R_e = 1.678R_d$), this becomes $r_c = 2.94\,R_d$.

free parameter. Importantly, the factor 2.94 cannot be significantly larger as there is not enough energy from supernovae to create cores of size much larger than $2.94\,R_d$ (see also e.g. Benítez-Llambay et al. 2019; Lazar et al. 2020; Trujillo-Gomez et al. 2021). The degree of transformation from cusp to core is described by the parameter n, with $n = 0$ defining a cuspy NFW profile and $n = 1$ a completely cored profile. The parameter n is defined as $n = \tanh(\kappa t_{\mathrm{SF}}/t_{\mathrm{dyn}})$, with $\kappa = 0.04$ a fixed parameter, t_{SF} the time whilst the galaxy has been forming stars (set to 14 Gyr), and t_{dyn} the NFW dynamical time at the scale radius r_s, which can be expressed in terms of M_{NFW}, r_s, and G (the Newtonian gravitational constant) as

$$t_{\mathrm{dyn}} = 2\pi \sqrt{\frac{r_s^3}{G M_{\mathrm{NFW}}(< r_s)}}. \tag{6}$$

The dark matter profile has then the same two free parameters as an NFW halo: the mass of the halo (M_{200}) and its concentration (c_{200}). *N*-body cosmological simulations find a strong correlation between c_{200} and M_{200} (e.g. Dutton & Macciò 2014; Ludlow et al. 2014), so in practice one can even fit NFW-like profiles with one single parameter. While the other parameters of the halo (n, r_s, r_c), are not considered free parameters, they also change on each step of our MCMC fitting (see below), as they depend on M_{200} and c_{200} as described above.

To find the best-fitting CDM halo, we use an MCMC routine (also based on emcee) that minimizes the residuals of equation (2) using a standard $\exp(-0.5\chi^2)$ function as likelihood, with χ^2 given by

$$\chi^2 = \sum \frac{(V_c - V_{c,\mathrm{mod}})^2}{\delta_{V_c}^2}, \tag{7}$$

where V_c and $V_{c,\mathrm{mod}}$ are the observed and model circular speed profiles, respectively, and δ_{V_c} is the [3D]Barolo uncertainty in the kinematic modelling, which we assume to be Gaussian (see Di Teodoro 2015). As we discuss next, the inclination is a free parameter in our MCMC, and thus δ_{V_c} itself does not include the contribution from the inclination uncertainty; these error bars are therefore smaller than those shown in Figs 3 and 4.

The MCMC explores the (M_{200}, c_{200}) parameter space and retrieves the best-fitting combination. In addition to M_{200} and c_{200}, we include the distance D and the inclination i as nuisance parameters. In practice, we impose a Gaussian prior on D centred at 76 Mpc and with a standard deviation of 5 Mpc, exploring the 2σ range $66 \leq D/\mathrm{Mpc} \leq 86$. Similarly, for i, we impose a Gaussian prior centered at $32°$ with a standard deviation of $3°$, within $26° \leq i \leq 38°$; in Section 5, we also discuss the case where the priors for D and i are wider. It is worth pointing out that a change in D introduces a change in the conversion factor between arcsecond and kpc, thus modifying our sampling of the rotation curve. Additionally, it affects the value of R_d, which in turn changes r_c and the thickness of the stellar disc. On the other hand, i affects the overall normalization of the rotation curve and of the gas circular speed profile. Having established this, we explore different scenarios, which differ by our chosen priors on M_{200} and c_{200}.

In a very first attempt, we use the flat priors $6 \leq \log(M_{200}/\mathrm{M}_\odot) \leq 12$ and $0.1 \leq c_{200} \leq 30$. However, c_{200} remains completely unconstrained as its posterior distribution is flat over all the explored range. Upon imposing the $c_{200}-M_{200}$ relation of Dutton & Macciò (2014) as a Gaussian prior on c_{200}, we find $\log(M_{200}/\mathrm{M}_\odot) = 7.6^{+0.7}_{-1.0}$, $c_{200} = 21^{+5}_{-3}$, $D = (76 \pm 5)$ Mpc, and $i = 33 \pm 3°$.

While the resulting fit is close to the data (given that $V_{\mathrm{bar}} \approx V_c$ and V_{DM} is subdominant), the value of $M_{200} \sim 10^8\,\mathrm{M}_\odot$ is too low to be plausible in a CDM cosmology. Given $M_{\mathrm{bar}} = 1.4 \times 10^9\,\mathrm{M}_\odot$,

the minimum expected M_{200} (assuming the galaxy has a baryon fraction as high as the cosmological average: $f_{c,bar} \simeq 0.16$, see Cimatti, Fraternali & Nipoti 2019) is about 0.9×10^{10} M$_\odot$. It is clear that the MCMC routine finds a low mass since $V_c \simeq V_{bar}$, but the resulting halo does not seem to have a physical justification.

Taking the above into consideration, we decided to impose a lower boundary to the prior of M_{200} such that the minimum halo would produce $M_{bar}/M_{200} \simeq 0.16$ (i.e. the cosmological baryon fraction). With this, the prior for M_{200} becomes $10 \leq \log(M_{200}/M_\odot) \leq 12$. We stress that the lower limit on the prior corresponds to the minimum expected value of M_{200}. In theory one expects the galaxy to have a significantly larger M_{200}. For example, the ΛCDM stellar-to-halo mass relation from Posti et al. (2020) would predict $\log(M_{200}/M_\odot) \approx 10.6$. For c_{200} we explore two scenarios: one where we impose again the $c_{200}-M_{200}$ relation of Dutton & Macciò (2014) as a Gaussian prior in the MCMC routine, and one where c_{200} has a flat wide prior $0.1 \leq c_{200} \leq 30$. In what follows, we refer to these two scenarios as Case 1 and Case 2, respectively.

The posterior distributions of both Case 1 and Case 2 are shown in Appendix B. Somewhat unsurprisingly, for both cases the MCMC finds $\log(M_{200}/M_\odot) \simeq 10$, with posterior distributions that simply try to go to the lower bound. In Case 1 (imposing the Gaussian prior on the $c_{200}-M_{200}$ relation), we find $D = (67 \pm 1)$ Mpc and $i = 26.1^{+0.2}_{-0.1}$, with posterior distributions also trying to go towards their lower bounds (see Fig. B2). The concentration, on the other hand, is well constrained, and we find $c_{200} = 11.7 \pm 0.3$. The other parameters of the CORENFW profile are $n = 0.7$, $r_c = 4.6$ kpc, and $r_s = 3.8$ kpc.

For Case 2, while D and i are well constrained following their priors ($D = 73 \pm 4$ Mpc, $i = 29° \pm 2°$), the posterior distribution of c_{200} goes to its lower bound, $c_{200} = 0.3^{+0.3}_{-0.2}$ (see Fig. B3). The other parameters of the CORENFW profile are $\log(M_{200}/M_\odot) = 10.2$, $n = 0.03$ (i.e. CORENFW $\approx$ NFW) driven by a high t_{dyn} (equation (6)), $r_c = 5.1$ kpc, and $r_s = 166$ kpc, driven by the extremely low c_{200} ($r_s = r_{200}/c_{200}$).

Fig. 5 shows the two resulting mass models. Case 1, on the left-hand panel, is in clear disagreement with the data as it significantly overestimates V_c, even when the distance and inclination go to their lowest allowed values. Case 2, on the right-hand panel, lies closer to the data but presents other problems, as we discuss in the next section.

5 DISCUSSION

Having presented our main results, we now discuss their implications. Provided our rotation curve for AGC 114905 faithfully traces its circular speed, the fact that it is baryon-dominated out to the outermost observed radius (Fig. 4) implies two possible scenarios is a ΛCDM context: that our UDG lacks a significant amount of dark matter across all radii (even beyond the range probed by our data), or that it has a peculiar dark matter halo with little mass within 10 kpc (e.g. right-hand panel in Fig. 5).

5.1 AGC 114905 compared to 'dark matter free' galaxies

Since van Dokkum et al. (2018, 2019) postulated that DF-2 and DF-4 have very low or no dark matter content, different mechanisms to create such peculiar galaxies have been proposed. One of the leading ideas is that high-velocity (~ 300 km s^{-1}) collisions between gas-rich dwarf galaxies can create dark matter free (or almost dark matter free, $M_{DM} \sim 10^5$ M$_\odot$) galaxies (Silk 2019; Shin et al. 2020). Importantly, those types of galaxies are expected to form in dense environments and to have a baryonic mass dominated by stars rather

than cold gas. Another mechanism proposed to explain the existence of DF-2 and DF-4 are tidal interactions with massive neighbouring galaxies that strip the dark matter away (Doppel et al. 2021; Jackson et al. 2021); Montes et al. (2020) claim that in fact DF-4 currently shows signs of such interactions.

While the above scenarios can manage to produce dark-matter poor, UDG-like galaxies that show some degree of similarity with DF-2 and DF-4, it is important to bear in mind that gas-rich UDGs are rather different objects. Not only they are gas-dominated ($f_{gas} \simeq 0.9$ for AGC 114905), but they are also isolated (by selection, see Leisman et al. 2017). In the specific case of AGC 114905, the nearest galaxy within a recession velocity of 500 km s^{-1} with confirmed (optical or H I) redshift, is the faint dwarf AGC 114806 at a projected distance of 2.1 Mpc and with a systemic velocity within a few km s^{-1}. Using data from the Sloan Digital Sky Survey (Alam et al. 2015), we also looked for possible unconfirmed massive companions of AGC 114905. We explored the area within 45 arcmin of AGC 114905, corresponding to a circle of radius 1 Mpc at the distance of AGC 114905, querying for galaxies with $R_e \geq 1$ kpc and with colour $(g - r) \leq 1$ mag. In this region, there are only seven galaxies with $M_* \gtrsim 10^9$ M$_\odot$ (assuming a distance of 76 Mpc and the mass-to-light–colour relation from Du et al. 2020) with unknown distance. All of them resemble confirmed background red galaxies, and the closest in projection lies at 700 kpc. All this evidence, together with the lack of tidal features in the optical and H I morphology of our UDG, suggests that it is truly isolated.

An idea that could reconcile a tidal origin with the current isolation of AGC 114905 is that it is an old tidal dwarf galaxy (TDG; e.g. Duc et al. 2014), since TDGs are expected to have a low dark matter content and low rotation velocities (e.g. Hunter, Hunsberger & Roye 2000; Lelli et al. 2015). If the interaction that originated the TDG happened at high redshift ($z \sim 4-6$) and the galaxy had an escape velocity of ~ 400 km s^{-1}, the parent galaxy would lie today at distances about ~ 5 Mpc from AGC 114905. While this scenario is impossible to test in practice, the population of known old TDGs in the nearby Universe both in observations and simulations are found at much closer distances and recessional velocities from their parent galaxies than what AGC 114905 (and the similar gas-rich UDGs from Mancera Piña et al. 2019b, 2020) is from any massive galaxy (Hunter et al. 2000; Kaviraj et al. 2012; Duc et al. 2014; Haslbauer et al. 2019). Overall, while is difficult to give a final answer, it seems unlikely that the small (if any) amount of dark matter in AGC 114905 can be attributed to the above-mentioned mechanisms perhaps valid for DF-2 and DF-4.

Recently, Trujillo-Gomez et al. (2021) proposed a semi-empirical model where strong feedback from globular clusters can produce UDGs with dark matter cores as large as 10–30 kpc. However, the model does not include a detailed treatment of the gas component that is the dominant mass budget of gas-rich UDGs, and a thorough comparison with our data is not yet possible to carry out.

It would be instructive to obtain information about the kinematics of AGC 114905 beyond 10 kpc, where the contribution of stars and gas becomes smaller and would produce a declining rotation curve. Instead, if a flat rotation curve were to be found, it would suggest the presence of dark matter. In the next section, motivated by our results in Fig. 5, we discuss which type of CDM haloes are in agreement or disagreement with our observations.

5.2 The c_{200} of a CDM halo for AGC 114905 is too low

It follows from Fig. 5 that it does not seem possible to fit the circular speed profile of AGC 114905 with a CDM-motivated c_{200}.
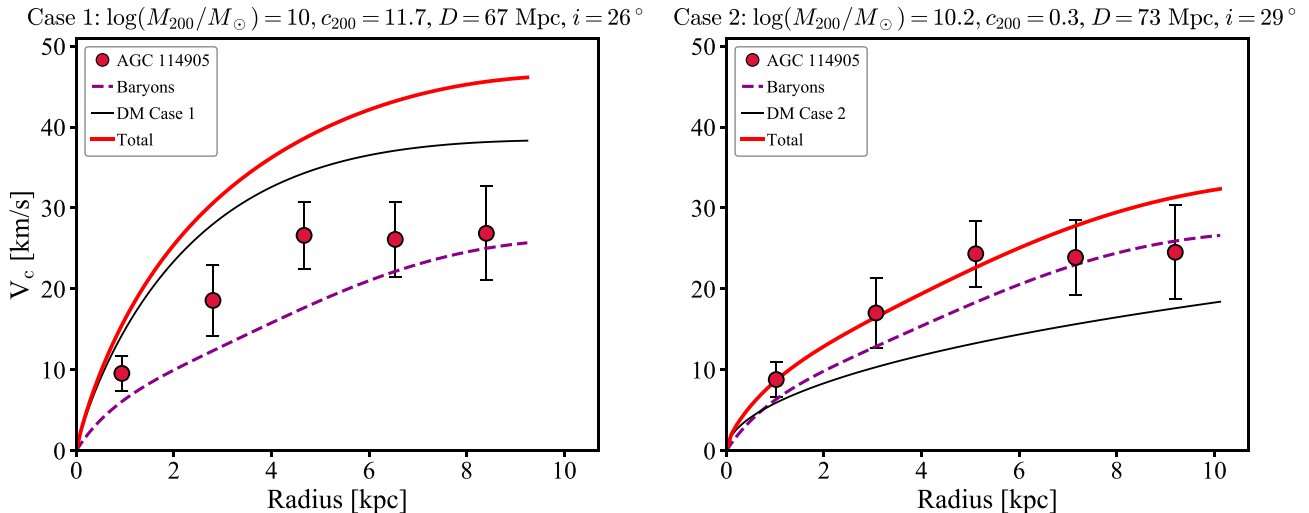
Figure 5. Mass models of AGC 114905. Case 1 and Case 2 are shown on the left-hand and right-hand panels, respectively. In both panels, the red points show the V_c profile of AGC 114905, while the dashed magenta lines represent the V_c expected from the baryons (stars plus gas). The dark matter haloes are shown with black lines, and the red lines give the total contribution of baryons and dark matter together. Case 1, which follows the CDM $c_{200}-M_{200}$ relation, is inconsistent with the observations. Case 2 fits the data better, but it has a c_{200} too low for CDM. Note also that the assumed distance and inclination are different between both panels. Because the assumed distance is different on each panel, the sampling of the rotation curve along the horizontal axes is also different. In a similar way, the normalization of the rotation curves differ from each other due to the different inclinations. See the text for details.

As mentioned above, if the $c_{200}-M_{200}$ relation is imposed (Case 1, left-hand panel of Fig. 5), it fails by a large margin at reproducing the amplitude of the circular speed profile. Case 2 (right-hand panel of Fig. 5), fitting a free c_{200}, does a better job and it is consistent with the circular speed profile within the uncertainties. However, c_{200} is too low and completely off the expected $c_{200}-M_{200}$ relation that emerges from cosmological simulations[7] (e.g. Dutton & Macciò 2014; Ludlow et al. 2014) and it might even be non-physical: McGaugh, Barker & de Blok (2003) argue that CDM haloes with $c_{200} < 2$ are not produced in any sensible cosmology. Sengupta et al. (2019) and Shi et al. (2021) also suggested that the gas-rich UDGs AGC 242019 and UGC 2165, respectively, have a c_{200} around 2. Drawing conclusions from those galaxies might be less straightforward: the rotation curve of AGC 242019 does not seem to reach its flat part, while the data of UGC 2165 have low resolution and its rotation curve (apparently rising as solid-body) is significantly oversampled. Still, it is interesting that similarly low values of c_{200} are reported.

It is important to highlight that while low surface brightness galaxies have been historically found to inhabit low-concentration haloes (e.g. McGaugh et al. 2003), the concentrations of those haloes are still usually in broad to good agreement with ΛCDM cosmology (Macciò et al. 2007), while the concentration of AGC 114905 is rejected at a high significance level. Given the volume explored by Leisman et al. (2017) when building the parent sample of AGC 114905 ($\sim 10^6$ Mpc^3, see Haynes et al. 2018; Jones et al. 2018), finding a single galaxy with the properties of AGC 114905 should be practically impossible in a CDM Universe. This result becomes even stronger considering the rest of the sample studied in Mancera Piña et al. (2019b, 2020) possibly shows similar properties, even

if slightly less extreme as AGC 114905 presents the largest offset from the BTFR. In this context, it is important to bear in mind that gas-rich UDGs as a whole population have significantly narrower velocity widths (a proxy for their rotation velocities) than galaxies of similar mass (Leisman et al. 2017; Jones et al. 2018).

We also note here that the implausibility of the CDM halo needed in AGC 114905 is not just related with the cusp-core problem (Bullock & Boylan-Kolchin 2017), since by fitting a CORENFW profile we do not force the halo to be cored or cuspy per se. It is also clear that the scales at which dark matter is deficient in AGC 114905 (10 kpc) are larger than any realistic core size for dwarf galaxies in both observations and simulations (e.g. Read et al. 2016a, 2017; Lazar et al. 2020). To further explore this, we performed a run of our MCMC routine where r_c is kept as a free parameter. In practice, we use a flat prior exploring the range $0 \leq r_c/\text{kpc} \leq 44$. The maximum value of 44 kpc is chosen because it is the value of r_{200} given $M_{200} = 10^{10}$ M$_\odot$. Additionally, we impose a minimum value on the prior of M_{200}, $\log(M_{200}/\text{M}_\odot) = 10$, as well as the Gaussian prior on the $c_{200} - M_{200}$ relation. The MCMC routine finds the parameters $\log(M_{200}/\text{M}_\odot) \approx 10^{10}$, $c_{200} \approx 12$, $D \approx 71$ Mpc, $i \approx 27°$, and $r_c \approx 41$ kpc, with the i and r_c posterior distributions simply going to their minimum and maximum allowed values, respectively. While the fit is just slightly worse than Case 2 (right-hand panel of Fig. 5) it seems non-physical. Expressing the core radius as $r_c = \eta R_e$ implies $\eta \sim 15$. As discussed by Read et al. (2017), there is not enough supernovae energy in galaxies to drive $\eta > 2.75$, and $\eta = 1.75$ fits real and simulated galaxies well. Even if other energy sources (e.g. Cimatti et al. 2019) can affect the distribution of dark matter in galaxies, it seems unlikely that they would contribute much more than supernovae, as required to achieve $r_c \approx r_{200}$.

Finally, it is worth clarifying that the problem of fitting a CDM halo to AGC 114905 is not restricted to specific functional forms such as the CORENFW profile. In addition to CORENFW, we also try with the COREEinasto halo, which allows the Einasto profile to develop a core, and which has been found by Lazar et al. (2020) to

---

[7]Assuming that the scatter of the $c_{200}-M_{200}$ relation measured at high masses ($\sigma_{\log(c_{200})}$ = 0.11 dex, see Dutton & Macciò 2014) is applicable also at $M_{200} \lesssim 10^{10}$ M$_\odot$, then c_{200} of AGC 114905 is about 15σ below the expected value, although this number could be reduced if the $c_{200}-M_{200}$ or its scatter depart from Gaussian (Kong et al., in preparation).

successfully reproduce the cored dark matter profile of a variety of galaxies in the FIRE-2 simulations (Hopkins et al. 2018). For this profile we also impose a minimum $\log(M_{200}/M_\odot) = 10$, but the only way to find agreement with our data is again if the size of the core is as large as r_{200}.

Overall, the existence of galaxies like AGC 114905 seems to pose a major challenge for CDM haloes. An interesting line of research is to explore whether or not the current issues can be mitigated by invoking a different type of dark matter (e.g. Kaplinghat, Ren & Yu 2020; Yang, Yu & An 2020).

5.3 AGC 114905 challenging MOND

Modified Newtonian dynamics (MOND; Milgrom 1983; Sanders & McGaugh 2002) is an alternative approach to dark matter theories which aims to explain dark matter physics by invoking a modification to Newtonian dynamics. One of the major achievements of MOND is how well it predicts rotation curves of galaxies (e.g. Sanders & McGaugh 2002; Famaey & McGaugh 2012 and references therein). Rather than a fit, MOND makes a direct prediction of the shape of the rotation curve given the stellar and gas mass distributions. The only other parameter is $a_0 \simeq 1.2 \times 10^{-8}$ cm s^{-2}, postulated to be a universal constant.

The fact that some isolated UDGs are off the BTFR already posed a challenge to MOND, which predicts a tight (zero intrinsic scatter) BTFR with slope of four for isolated galaxies. Yet, some doubts about this may exist, as it could be argued that the circular speeds reported in Mancera Piña et al. (2019b, 2020) were not tracing the flat part of the rotation curve or were too affected by the resolution; here, we have shown that this is not the case for AGC 114905.

Following Gentile (2008), in the absence of an 'external' gravitational field of a neighbouring massive galaxy, the MOND rotation curve can be written as

$$V_{MOND}^2(r) = V_{bar}^2 + \frac{V_{bar}^2}{2}\left(\sqrt{1 + \frac{4a_0 r}{V_{bar}^2}} - 1\right). \qquad (8)$$

We stress that the above formula is applicable to our UDG given the lack of massive galaxies in its vicinity. In order to test this prediction, we performed another MCMC fit with D and i as free parameters (which affect both V_c and V_{MOND}), following the same Gaussian priors as for our Case 1 and Case 2 above. Even with the posterior distributions for D and i going to their lower bounds ($D \approx 66$ Mpc and $i \approx 26°$, see Fig. B4 in Appendix B), the MOND prediction markedly overestimates the circular speed of our UDG (consistent with the offset from the BTFR), as we show in Fig. 6. There may be also some tension with the shape of the rotation curve, which is not predicted to be flat as in the observations. Therefore, our UDG seemingly presents a challenge to MOND, which can only be reconciled by invoking a much lower inclination, as we discuss in Section 5.4.

5.4 The effects of a lower inclination

As described in Section 3, we measure the inclination of AGC 114905 to be $32° \pm 3°$, using a well-tested method that relies exclusively on the total H I map and is independent of the kinematics of the galaxy and our posterior kinematic modelling. While we argue that our inclination is robust, our results are certainly dependent on it. In particular, if AGC 114905 had a much lower inclination, the amplitude of its rotation curve would be significantly larger, having more room for dark matter within the observed radii and potentially
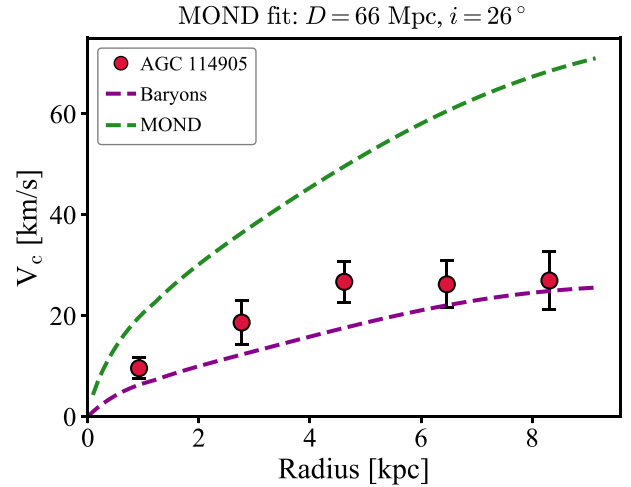

Figure 6. MOND prediction (green line) of the circular speed profile of AGC 114905 (red points). The baryonic circular speed profile is shown with a magenta line.

alleviating some of the tensions presented in this paper (see for instance the case of IC 1613 in Oman et al. 2016).

Given this, it is interesting to quantify by how much the inclination of our UDG would need to decrease to make it consistent with the CDM (and MOND) expectation. For this exploration we assume a CORENFW profile with $r_c = 2.94\, R_d$. The 'minimum' expectation is such that the galaxy has $\log(M_{200}/M_\odot) = 10$ and a c_{200} in agreement (within some scatter) with the $c_{200}-M_{200}$ relation. We run again our MCMC routine, but this time we use wider Gaussian priors for D and i: $50 \leq D/\text{Mpc} \leq 100$ and $5° \leq i < 85°$, with centre and standard deviations as in Case 1. The resulting parameters are $\log(M_{200}/M_\odot) = 10.03^{+0.06}_{-0.03}\, M_\odot$, $c_{200} = 12.1 \pm 0.3$, $D = (72.7 \pm 5)$ Mpc, and $i = (15 \pm 1)°$. The low inclination brings up the circular speed of AGC 114905 to velocities around 45 km s^{-1}, which are consistent with a CORENFW halo similar to the halo in Case 1 (the other parameters are $n = 0.73$, $r_c = 5$ kpc, and $r_s = 3.8$ kpc).

With an inclination of $15°$ the galaxy would be still quite puzzling, as it would have a baryon fraction about 70 per cent the value of the cosmological average (90 per cent if $D = 76$ Mpc), as opposed to most dwarf galaxies that have low baryon fractions of a few per cent (McGaugh et al. 2010; Read et al. 2017). Additionally, AGC 114905 would still lie off the BTFR. If one instead imposes $\log(M_{200}/M_\odot) = 10.6$ (which gives a baryon fraction of about 20 per cent) assuming the ΛCDM stellar-to-halo mass relation from Posti et al. (2020), a corresponding $c_{200} = 11.5$ (following the $c_{200}-M_{200}$ relation), and $D = 76$ Mpc, the needed inclination is $10.4 \pm 0.3°$. Similarly, an inclination of $i = 10.8 \pm 0.3°$ would be needed in order to find agreement between the MOND prediction and the V_c profile of AGC 114905, at least on average, since the shape predicted by MOND seems to also differ from our rotation curve. Note, however, that a radially varying inclination could potentially alleviate this tension between the rotation curves shapes.

The above values for the inclination are about $20°$ off the inclination we determined in Section 3. This is a discrepancy a factor 6–7 larger than the nominal uncertainty estimate of our measurement (see Fig. B1), although inclinations below $\sim 25°$ become increasingly difficult to constrain as ellipses with lower inclinations all have very similar shapes. We can also inspect visually if inclinations as low as $11°-15°$ can be consistent with the data. In Fig. 7, we show the outer contour of the H I map of AGC 114905 overlaid on the r-band
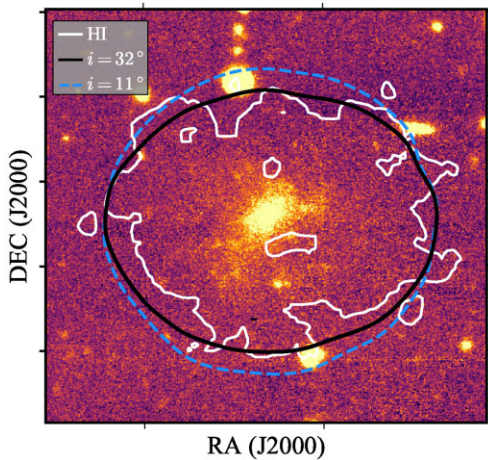
Figure 7. Comparison between the outer contours (S/N = 3) of the H I map of AGC 114905 (white) and two azimuthal models at different inclinations. While the model at 32° (solid black line) provides a good fit to the data, the model at 10° (dashed blue) is significantly more elongated than the data along the minor axis. The background shows the optical image of AGC 114905.

optical image, and we compare it with the equivalent contours of two ³ᴰBarolo azimuthal models (convolved with the observed beam) of AGC 114905 at different inclinations. The models are razor-thin axisymmetric discs (but see Section 3.1). The model at 32° does an overall good job at following the H I contour, while the contour for the model at 11° appears inconsistent with it, being significantly more elongated along the minor axis. This is also shown in Fig. A1 where we compare the channel maps of AGC 114905 with the channel maps of our best-fitting model and those of a model with an inclination of 11°.

Given all of the above, we find it unlikely that we are severely overestimating the inclination of our UDG, although this remains the largest source of uncertainty in our analysis. Something else to consider is that there are other gas-rich UDGs showing a similar set of properties, all at different inclinations (Mancera Piña et al. 2019b, 2020, see also Sengupta et al. 2019; Shi et al. 2021, and the spatially unresolved data from e.g. Leisman et al. 2017; Karunakaran et al. 2020; Guo et al. 2020). This means that the inclinations of all of them would need to be overestimated by a large margin. Still, it is desirable to repeat our analysis with a gas-rich UDG at a similar resolution as we have now for AGC 114905, but at higher inclination, and we aim to do this in the near future.

6 CONCLUSIONS

We obtained new H I interferometric observations of the gas-rich ultra-diffuse galaxy (UDG) AGC 114905 using the Karl G. Jansky Very Large Array in its B-, C- and D-configurations. The new data, tracing the H I emission up to 10 kpc from the galaxy centre, have a spatial resolution a factor about 2.5 higher than previous data, and confirm that AGC 114905 has a regularly rotating gas disc.

We performed 3D kinematic modelling of the data cube using ³ᴰBarolo, which allowed us to recover the intrinsic rotation curve and velocity dispersion profile of the galaxy. AGC 114905 has a regular rotation curve that reaches a flat part with a circular speed (after a minor correction for asymmetric drift) of about 23 km s⁻¹. This result confirms that this UDG lies off the baryonic Tully–Fisher relation, as suggested by Mancera Piña et al. (2019b, 2020) with low-resolution data.

The observed circular speed profile of our UDG can be explained almost entirely by the contribution of the baryons alone, with little room for dark matter within our observed outermost radius (R ≈ 10 kpc). Moreover, we found that the circular speed profile cannot be reproduced by standard CDM haloes: the only possibility to find a good fit to the data is if the concentration of the halo is as low as ∼0.3, completely off CDM expectations. We tested whether the rotation of our UDG is instead reproduced within the MOND framework, but we find that there is a significant mismatch on the normalization and shape of the MOND rotation curve with respect to our observations.

The geometry of the system (assumed to be an inclined axisymmetric disc) is the main source of uncertainty in our results. The inclination of AGC 114905 (32 ± 3°), which we measure from its total H I map independently of its kinematics, is a significant caveat, but a number of independent pieces of evidence suggest that it cannot be overestimated to the extent of significantly changing the above results. Efforts to observe another gas-rich UDG at a similar spatial resolution but at higher inclination are under way. Finally, it is important to consider that we have confirmed for one UDG the robustness of the results obtained by Mancera Piña et al. (2019b, 2020) at low resolution. The fact that the six UDGs (and see also e.g. Leisman et al. 2017; Shi et al. 2021) at different inclinations show the same behaviour argues in favour of them being really exotic and suggests that our results are not the byproduct of systematic uncertainties.

We have strengthened and clarified previous results on the nature and startling dynamics of gas-rich UDGs. Yet, their origin and precise evolutionary pathways remain largely a mystery. This work has also shown that gas-rich UDGs are a promising population to study dark matter, as they can potentially provide telltale clues to understand its nature.

DATA AVAILABILITY

The data sets generated during and/or analysed during the current study are available from the corresponding author on reasonable request.

REFERENCES

Alam S. et al., 2015, ApJS, 219, 12

Amorisco N. C., Loeb A., 2016, MNRAS, 459, L51

Astropy Collaboration, 2018, AJ, 156, 123

Bacchini C., Fraternali F., Pezzulli G., Marasco A., 2020, A&A, 644, A125

Barbosa C. E. et al., 2020, ApJS, 247, 46

Begeman K. G., 1987, PhD thesis, Kapteyn Astronomical Institute, University of Groningen

Benítez-Llambay A., Frenk C. S., Ludlow A. D., Navarro J. F., 2019, MNRAS, 488, 2387

Bershady M. A., Verheijen M. A. W., Westfall K. B., Andersen D. R., Swaters R. A., Martinsson T., 2010, ApJ, 716, 234

Bosma A., 1978, PhD thesis, University of Groningen

Bullock J. S., Boylan-Kolchin M., 2017, ARA&A, 55, 343

Carleton T., Errani R., Cooper M., Kaplinghat M., Peñarrubia J., Guo Y., 2019, MNRAS, 485, 382

Chamba N., Trujillo I., Knapen J. H., 2020, A&A, 633, L3

Chan T. K., Kereš D., Wetzel A., Hopkins P. F., Faucher-Giguère C. A., El-Badry K., Garrison-Kimmel S., Boylan-Kolchin M., 2018, MNRAS, 478, 906

Cimatti A., Fraternali F., Nipoti C., 2019, Introduction to Galaxy Formation and Evolution: From Primordial Gas to Present-Day Galaxies. Cambridge Univ. Press, Cambridge

Conselice C. J., 2018, Res. Notes Am. Astron. Soc., 2, 43

Danieli S., van Dokkum P., Conroy C., Abraham R., Romanowsky A. J., 2019, ApJ, 874, L12

de Blok W. J. G., Walter F., Brinks E., Trachternach C., Oh S. H., Kennicutt R. C. J., 2008, AJ, 136, 2648

Di Cintio A., Brook C. B., Dutton A. A., Macciò A. V., Obreja A., Dekel A., 2017, MNRAS, 466, L1

Di Teodoro E. M., 2015, PhD thesis, University of Bologna

Di Teodoro E. M., Fraternali F., 2015, MNRAS, 451, 3021

Di Teodoro E. M., Fraternali F., Miller S. H., 2016, A&A, 594, A77

Doppel J. E., Sales L. V., Navarro J. F., Abadi M. G., Peng E. W., Toloba E., Ramos-Almendares F., 2021, MNRAS, 502, 1661

Du W., Cheng C., Zheng Z., Wu H., 2020, AJ, 159, 138

Duc P.-A., Paudel S., McDermid R. M., Cuillandre J.-C., Serra P., Bournaud F., Cappellari M., Emsellem E., 2014, MNRAS, 440, 1458

Dutton A. A., Macciò A. V., 2014, MNRAS, 441, 3359

Elmegreen B. G., Hunter D. A., 2015, ApJ, 805, 145

Emsellem E. et al., 2019, A&A, 625, A76

Famaey B., McGaugh S. S., 2012, Living Rev. Relativ., 15, 10

Fattahi A. et al., 2016, MNRAS, 457, 844

Foreman-Mackey D., 2016, J. Open Source Softw., 1, 24

Foreman-Mackey D., Hogg D. W., Lang D., Goodman J., 2013, PASP, 125, 306

Fraternali F., Karim A., Magnelli B., Gómez-Guijarro C., Jiménez-Andrade E. F., Posses A. C., 2021, A&A, 647, A194

Gault L. et al., 2021, ApJ, 909, 19

Gentile G., 2008, ApJ, 684, 1018

Ginsburg A. et al., 2019, radio-astro-tools/spectral-cube: v0.4.4

Guo Q. et al. 2020, Nat. Astron., 4, 246

Haslbauer M., Dabringhausen J., Kroupa P., Javanmardi B., Banik I., 2019, A&A, 626, A47

Haynes M. P. et al., 2018, ApJ, 861, 49

Hidalgo-Gámez A. M., 2004, Rev. Mex. Astron. Astrofis., 40, 37

Hopkins P. F. et al., 2018, MNRAS, 480, 800

Hunter D. A., Elmegreen B. G., Baker A. L., 1998, ApJ, 493, 595

Hunter D. A., Elmegreen B. G., Berger C. L., 2019, AJ, 157, 241

Hunter D. A., Hunsberger S. D., Roye E. W., 2000, ApJ, 542, 137

Hunter J. D., 2007, Comput. Sci. Eng., 9, 90

Impey C., Bothun G., Malin D., 1988, ApJ, 330, 634

Iorio G., 2018, PhD thesis, alma, http://amsdottorato.unibo.it/8449/

Iorio G., Fraternali F., Nipoti C., Di Teodoro E., Read J. I., Battaglia G., 2017, MNRAS, 466, 4159

Jackson R. A. et al., 2021, MNRAS, 502, 1785

Jones M. G., Papastergis E., Pandya V., Leisman L., Romanowsky A. J., Yung L. Y. A., Somerville R. S., Adams E. A. K., 2018, A&A, 614, A21

Kado-Fong E. et al., 2021, ApJ, 920, 72

Kaplinghat M., Ren T., Yu H.-B., 2020, J. Cosmol. Astropart. Phys., 2020, 027

Karunakaran A., Spekkens K., Zaritsky D., Donnerstein R. L., Kadowaki J., Dey A., 2020, ApJ, 902, 39

Kaviraj S., Darg D., Lintott C., Schawinski K., Silk J., 2012, MNRAS, 419, 70

Laporte C. F. P., Agnello A., Navarro J. F., 2019, MNRAS, 484, 245

Lazar A. et al., 2020, MNRAS, 497, 2393

Leisman L. et al., 2017, ApJ, 842, 133

Lelli F. et al., 2015, A&A, 584, A113

Leroy A. K., Walter F., Brinks E., Bigiel F., de Blok W. J. G., Madore B., Thornley M. D., 2008, AJ, 136, 2782

Ludlow A. D., Navarro J. F., Angulo R. E., Boylan-Kolchin M., Springel V., Frenk C., White S. D. M., 2014, MNRAS, 441, 378

Macciò A. V., Dutton A. A., van den Bosch F. C., Moore B., Potter D., Stadel J., 2007, MNRAS, 378, 55

Mancera Piña P. E. et al., 2019b, ApJ, 883, L33

Mancera Piña P. E. et al., 2020, MNRAS, 495, 3636

Mancera Piña P. E., Aguerri J. A. L., Peletier R. F., Venhola A., Trager S., Choque Challapa N., 2019a, MNRAS, 485, 1036

Marasco A., Oman K. A., Navarro J. F., Frenk C. S., Oosterloo T., 2018, MNRAS, 476, 2168

McGaugh S. S., Barker M. K., de Blok W. J. G., 2003, ApJ, 584, 566

McGaugh S. S., Schombert J. M., Bothun G. D., de Blok W. J. G., 2000, ApJ, 533, L99

McGaugh S. S., Schombert J. M., de Blok W. J. G., Zagursky M. J., 2010, ApJ, 708, L14

Mihos J. C. et al., 2015, ApJ, 809, L21

Mihos J. C., McGaugh S. S., de Blok W. J. G., 1997, ApJ, 477, L79

Milgrom M., 1983, ApJ, 270, 365

Montes M., Infante-Sainz R., Madrigal-Aguado A., Román J., Monelli M., Borlaff A. S., Trujillo I., 2020, ApJ, 904, 114

Navarro J. F., Frenk C. S., White S. D. M., 1997, ApJ, 490, 493

Oliphant T. E., 2007, Comput. Sci. Eng., 9, 10

Oman K. A., Navarro J. F., Sales L. V., Fattahi A., Frenk C. S., Sawala T., Schaller M., White S. D. M., 2016, MNRAS, 460, 3610

Posti L., Famaey B., Pezzulli G., Fraternali F., Ibata R., Marasco A., 2020, A&A, 644, A76

Posti L., Pezzulli G., Fraternali F., Di Teodoro E. M., 2018, MNRAS, 475, 232

Read J. I., Agertz O., Collins M. L. M., 2016a, MNRAS, 459, 2573

Read J. I., Iorio G., Agertz O., Fraternali F., 2016b, MNRAS, 462, 3628

Read J. I., Iorio G., Agertz O., Fraternali F., 2017, MNRAS, 467, 2019

Román J., Beasley M. A., Ruiz-Lara T., Valls-Gabaud D., 2019, MNRAS, 486, 823

Román J., Trujillo I., 2017, MNRAS, 468, 4039

Romeo A. B., 1994, A&A, 286, 799

Romeo A. B., Falstad N., 2013, MNRAS, 433, 1389

Rong Y., Guo Q., Gao L., Liao S., Xie L., Puzia T. H., Sun S., Pan J., 2017, MNRAS, 470, 4231

Sales L. V., Navarro J. F., Peñafiel L., Peng E. W., Lim S., Hernquist L., 2020, MNRAS, 494, 1848

Sanders R. H., McGaugh S. S., 2002, ARA&A, 40, 263

Sault R. J., Teuben P. J., Wright M. C. H., 1995, in Shaw R. A., Payne H. E., Hayes J. J. E., eds, ASP Conf. Ser. Vol. 77, Astronomical Data Analysis Software and Systems IV. Astron. Soc. Pac., San Francisco, p. 433

Sawala T. et al., 2015, MNRAS, 448, 2941

Sengupta C., Scott T. C., Chung A., Wong O. I., 2019, MNRAS, 488, 3222

Shi Y., Zhang Z.-Y., Wang J., Chen J., Gu Q., Yu X., Li S., 2021, ApJ, 909, 20

Shin E.-J., Jung M., Kwon G., Kim J.-H., Lee J., Jo Y., Oh B. K., 2020, ApJ, 899, 25

Silk J., 2019, MNRAS, 488, L24

Swaters R. A., 1999, PhD thesis, Kapteyn Astronomical Institute, University of Groningen

Toomre A., 1964, ApJ, 139, 1217

Toomre A., 1981, in Fall S. M., Lynden-Bell D., eds, Structure and Evolution of Normal Galaxies. Cambridge University Press, Cambridge, p. 111

Tremmel M., Wright A. C., Brooks A. M., Munshi F., Nagai D., Quinn T. R., 2020, MNRAS, 497, 2786

Trujillo I. et al., 2019, MNRAS, 486, 1192

Trujillo-Gomez S., Kruijssen J. M. D., Reina-Campos M., 2021, MNRAS, in press, preprint (arXiv:2103.08610)

van der Burg R. F. J., Muzzin A., Hoekstra H., 2016, A&A, 590, A20

van der Hulst J. M., Terlouw J. P., Begeman K. G., Zwitser W., Roelfsema P. R., 1992, in Worrall D. M., Biemesderfer C., Barnes J., eds, ASP Conf. Ser. Vol. 25, Astronomical Data Analysis Software and Systems I. Astron. Soc. Pac., San Francisco, p. 131

van Dokkum P. et al., 2018, Nature, 555, 629

van Dokkum P. G., Abraham R., Merritt A., Zhang J., Geha M., Conroy C., 2015, ApJ, 798, L45

van Dokkum P., Danieli S., Abraham R., Conroy C., Romanowsky A. J., 2019, ApJ, 874, L5

Virtanen P. et al., 2020, Nat. Methods, 17, 261

Wang J., Yang K., Zhang Z.-Y., Fang M., Shi Y., Liu S., Li J., Li F., 2020, MNRAS, 499, L26

Wright A. C., Tremmel M., Brooks A. M., Munshi F., Nagai D., Sharma R. S., Quinn T. R., 2021, MNRAS, 502, 5370

Yang D., Yu H.-B., An H., 2020, Phys. Rev. Lett., 125, 111105

APPENDIX A: CHANNEL MAPS

Fig. A1 shows representative channel maps of the data cube of AGC 114905. The observed emission is shown in grey background and dark blue contours (open contours for negative values). The green cross shows the centre of the galaxy and the velocity of each channel map is given on the bottom right corner of each panel. In red, we show the contours for the best-fitting ^{3D}Barolo azimuthal tilted-ring model; while low S/N features are not fully reproduced, the model captures well the overall kinematics of the galaxy, as also shown in Fig. 2 with the PV diagrams. We also overlay in light blue the contours for a model with a fixed inclination of 11° (as needed to match CDM and MOND expectations, see Section 5.4). A close inspection shows that the model at 11° has an excess of flux along the minor axis in the channels close to the systemic velocity; the model at 32° does a better job in this regard (however, this comparison is better appreciated in Fig. 7). Moreover, the model at 32° matches in a better way the spectral extent of the observations.
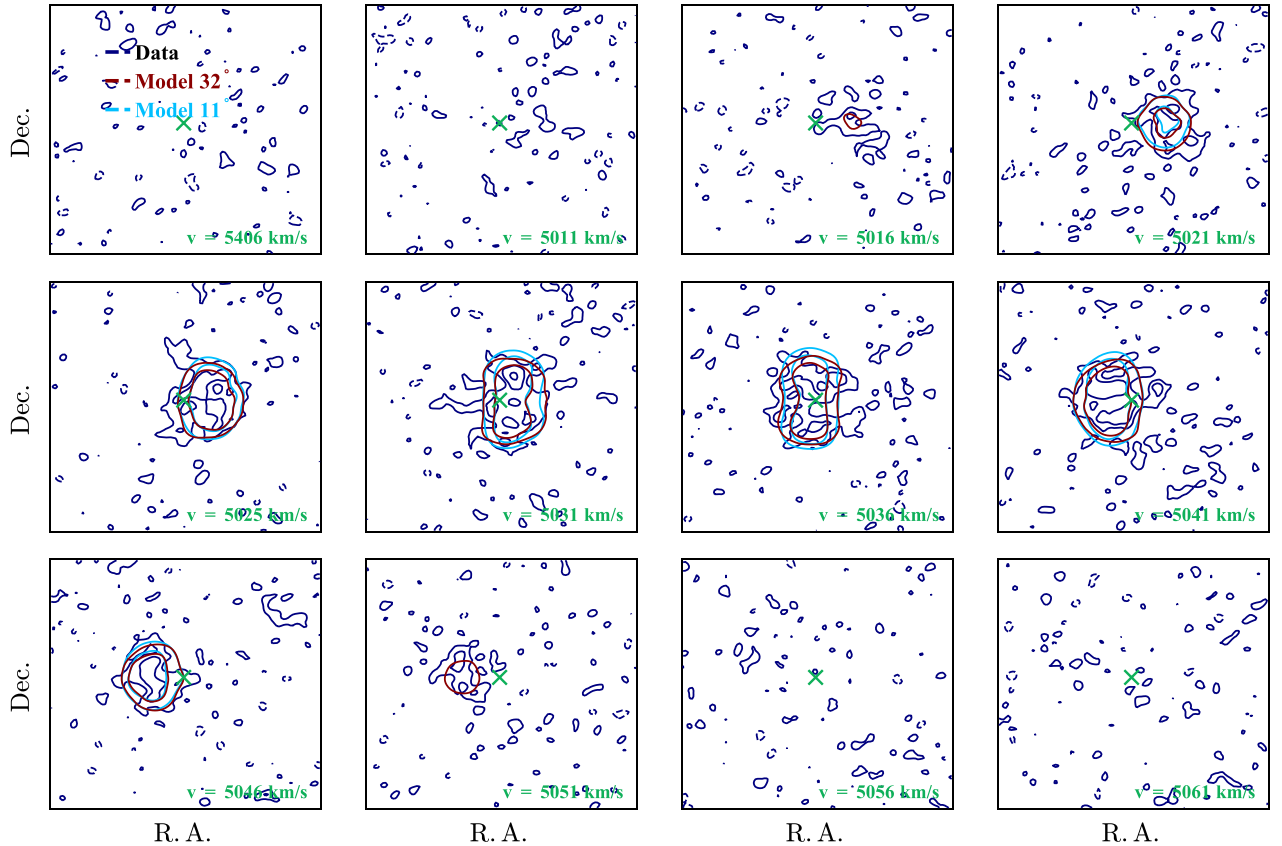
Figure A1. Representative channel maps of AGC 114905. The emission of the galaxy is shown in grey background and dark blue contours (open contours for negative values). The green crosses show the centre of the galaxy, and we indicate the velocity corresponding to each channel map on the bottom right corner. The contours for the best-fitting ^{3D}Barolo azimuthal tilted-ring model are shown in red, while the contours for a model at 11° are shown in light blue. Contours are at −2, 2, 4 times the rms noise per channel.
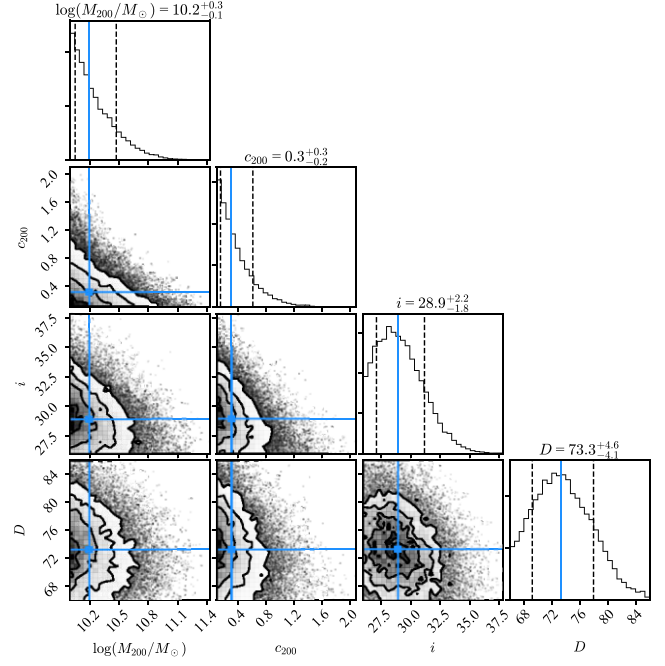
APPENDIX B: MCMC POSTERIOR DISTRIBUTIONS

In this appendix, we provide the main posterior distributions obtained with our MCMC analyses as described in the main text.
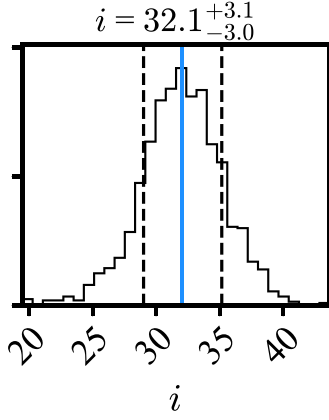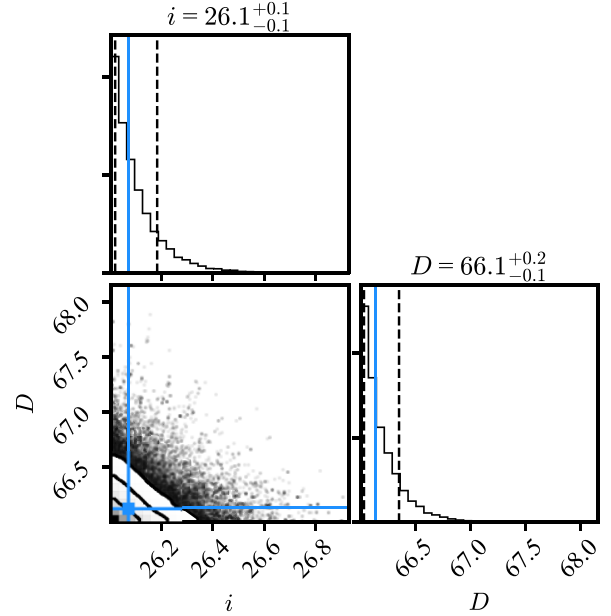
Figure B1. MCMC posterior distribution of the inclination of AGC 114905. The central value, shown in blue, is the median of the distribution, while the uncertainties represent the difference between the median and the 16th and 84th percentiles (dashed black lines). See Section 3.1 for details.
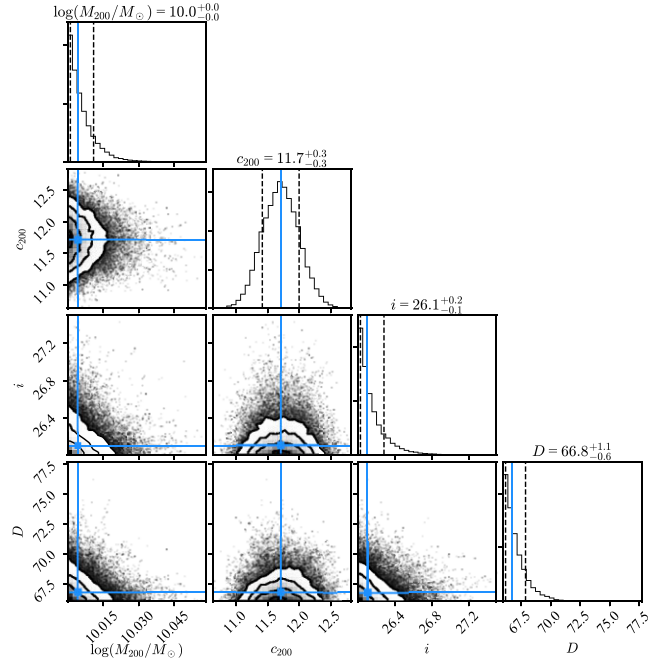
Figure B2. MCMC posterior distribution for our Case 1 mass model. Lines are as in Fig. B1. See Section 4 for details.

Figure B3. MCMC posterior distribution for our Case 2 mass model. Lines are as in Fig. B1. See Section 4 for details.

Figure B4. MCMC posterior distribution for the MOND model. Lines are as in Fig. B1. See Section 5.3 for details.

This paper has been typeset from a TEX/LATEX file prepared by the author.